Chinese Chemical Letters 36 (2025) 109784

Contents lists available at ScienceDirect

Chinese Chemical Letters

journal homepage: www.elsevier.com/locate/cclet

A dual-protease-triggered chemiluminescent probe for precise tumor imaging

Zhihui Zhang[a,1], Ru Sun[a,1], Chong Bian[b,1], Hongbo Wang[c], Zhen Zhao[b], Panpan Lv[b], Jianzhong Lu[a], Haixin Zhang[a], Hulie Zeng[a], Yuanyuan Chen[d], Zhijuan Cao[a,b,*]

[a] Department of Pharmaceutical Analysis, School of Pharmacy, Fudan University, Shanghai 201203, China
[b] Minhang Branch, Zhongshan Hospital, Fudan University, Shanghai 201199, China
[c] China State Institute of Pharmaceutical Industry, Shanghai 200040, China
[d] Shanghai Jahwa United Co., Ltd., Shanghai 200082, China

ARTICLE INFO

Article history:
Received 15 December 2023
Revised 9 March 2024
Accepted 15 March 2024
Available online 22 March 2024

Keyword:
Dual-protease imaging
Tripeptide substrate
Chemiluminescent
Phenoxy-dioxetane scaffold
Logic gates

ABSTRACT

Imaging detection of interlinked dual proteases is imperative for precise tumor imaging, which remains challenging due to limited modification position of specific substrate and possible steric hindrance. Herein, we have developed a unimolecular chemiluminescent probe (**LGP-CL**) tandemly activated by two proteases interlinked with liver cancer to achieve precise tumor imaging. Probe **LGP-CL** consists of a phenoxy-dioxetane scaffold caged by a tripeptide substrate (LGP, leucine-glycine-proline) as the sensing layer, which can be cleaved sequentially by aminopeptidase N (APN) and dipeptidyl peptidase IV (DPPIV) to turn on a strong chemiluminescent signal, and silenced by specific inhibitor of each enzyme, which accounts for an integrated logic gate (AND, OR and INHIBIT). The successful cleavage of dual proteases on the metabolic site depends on the proper structure of the tripeptide substrate, as confirmed by two probes design. Probe **LGP-CL** (LGP as the substrate) enables the excellent "dual-lock-dual-key" fit with a 382-fold enhancement of chemiluminescent emission while no obvious signal is observed by using **GPL-CL** (GPL as the substrate). By virtue of its rapid response (several minutes), high sensitivity and good cell viability, probe **LGP-CL** has been utilized to evaluate upregulated levels of proteases *in vitro* and in living systems, especially to distinguish liver tumor cells (HepG2) from others (LO2, MCF-7, MCF-10a and RAW264.7). Overall, the newly developed CL probe may facilitate rapid investigation into the role played by proteases in liver diseases, enabling timely selection appropriate treatment. Therefore, our work not only sheds light on the rational design of optical probes for dual protease imaging, but provides a promising tool for clinical diagnosis and even drug discovery.

Abnormal expression of multiple biomarkers [1], such as cellular microenvironment, small biomolecules, reactive oxygen species and various proteases have been implicated in many diseases. Particularly, proteases are involved in almost all biological and regulatory processes in living systems, which can be used as biomarkers of tumorigenesis and inflammatory immune responses and clinical targets for drug development [2]. More importantly, it is common for one disorder to include two or more interconnected proteases [3–5]. It is also demonstrated that low efficiency of curative therapy is mainly due to the lack of early and reliable diagnostic strategies [6]. To enhance the reliability, simultaneous detection of two or more correlated biomarkers with one disease is a promising way [6,7]. As reported, aminopeptidase N (APN, a zinc-dependent transmembrane peptidase) and dipeptidyl peptidase IV (DPPIV, CD26, a cell surface glycoprotein) were involved in various procession of liver diseases, such as liver cancer angiogenesis, metastasis and invasion, and chronic liver injury [8–10]. In view of the crosstalk of APN and DPPIV in liver diseases, a duplex/multiplex biosensor is promising to offer the precise diagnosis of liver diseases.

Various techniques have been developed for protease analysis [11–13], such as high-performance liquid chromatography (HPLC), liquid chromatography-mass spectrometry (LC-MS), immunoassay and optical methods. Optical molecular probes, especially activatable ones, are widely employed to monitor protease activity in living organisms due to their ability to offer the chemical and spatiotemporal information, easy operation, and noninvasiveness [14–17]. However, probes for sensing APN and DPPIV reported previously were single-locked with response to a single enzyme [18–20]. If

* Corresponding author.
E-mail address: zjcao@fudan.edu.cn (Z. Cao).
[1] These authors contributed equally to this work.

https://doi.org/10.1016/j.cclet.2024.109784
1001-8417/

Scheme 1. Proposed mechanism on dual-protease CL detection using a unimolecular probe.

combining their results to improve the reliability, it proved time- and cost-consuming and possibly showed different pharmacokinetics, penetration capabilities and metabolisms [21]. In further, dual-locked probes can offer duplex sensing capability along with enhanced selectivity by minimizing false-positive or false-negative results, thereby attracting continuous interest [7,22,23]. Unlike to detect two different types of targets (reactive oxygen species, acidic microenvironment, small biomolecules or enzymes) [24–26], dual-protease imaging was a big challenge due to the potential influence of multiple substrate modifications and steric hindrance on enzyme cleavage activity. To enable efficient analysis [27], two cleavage sites were strategically incorporated into different regions of coumarin skeleton, which required two modification or sensing positions within a single optical scaffold. In case where only one suitable site for modification exists, careful design of dual-locked probes is necessary to avoid interference and enhance enzymatic efficiency. Thus, these protocols with high sensitivity and specificity are still in urgent requirement.

To address this essue, chemiluminescence (CL) is selected due to its powerful ability in trace analysts, relying on its elimination of external light resource, thus low background and high sensitivity [28]. Until now, phenoxy-dioxetane scaffold-based CL probes have attracted increasing attention and been employed to establish one-step activatable imaging sensors with advantages of high emission under aqueous conditions, good cell permeability, and tunable "off-on" properties [29–34]. However, they are mainly single-locked ones. Herein, we propose a unimolecular CL probe for dual-protease imaging that tethers specific substrates targeting APN and DPPIV onto the phenoxy-dioxetane scaffold as the sensing layer. Only tandemly activated by both proteases, this CL probe can release intense CL light suitable for precise tumor imaging.

Our designed unimolecular probe incorporated cascade substrates (S_1 and S_2) of two proteases as the masking group onto the CL scaffold. The proposed mechanism behind the CL technique for dual protease imaging was elucidated in Scheme 1, probe (S_1S_2-CL) comprised three key domains: the recognition site (cascaded substrates for APN and DPPIV), a linker (a self-immolative spacer), and the CL scaffold (phenolated adamantly-1,2-dioxetane). Initially, the chemiexcitation energy of the probes was constrained by the cage group (tripeptide residue), resulting in no emission. Once the phenol masking group was sequentially removed by two proteases, followed by the subsequent cleavage of the self-immolative linker through 1,6-elimination, the chemiexcitation process was allowed to proceed *via* intramolecular chemically initiated electron exchange luminescence (CIEEL). This generated an unstable phenolate species that subsequently decomposed to form an excited benzoate ester, ultimately decaying to its ground state with green light emission.

For that, careful consideration was required in designing the amino acid sequences of the peptide substrates to achieve efficient activation and high sensitivity. This was due to the specific size and shape of enzymatic cavities and the intricate interactions between enzymes and their substrates. We hypothesized that even if potential substrates could fit into the active cavity of the enzyme like a key into a lock, the presence of additional amino acid residues might lead to steric hindrance and improper spatial conformation at the expected metabolic site of the CL probes. This could significantly limit their activation by the corresponding enzymes (Fig. 1a). To test our hypothesis, we designed and synthesized two probes, **LGP-CL** and **GPL-CL** (Fig. 1b), each containing an individual tripeptide sequences (Leu-Gly-Pro and Gly-Pro-Leu respectively) as the recognition site, followed by the linkage with a self-immolative spacer and CL scaffold (Figs. S1–S3, detailed synthesis, purification and characterization procedures seen in Supporting information) [17]. Then, we compared the ability of two probes *in vitro* detection for dual proteases. As shown in Fig. 1b, **GPL-CL** produced no obvious CL signal enhancement after addition of APN (100 U/L) and DPPIV (1 μg/mL). By contrast, probe **LGP-CL** was triggered to generate a strong CL emission with a remarkable 382-fold enhancement.

Subsequently, we recorded the CL kinetic curves using Thermo Scientific™ Fluoroskan FL in the presence of both proteases, showing a rapid, time-dependent signal increase lasting for up to 3 h (Fig. 1c, green line). Crucially, no significant CL signal was observed when APN and DPPIV were separately employed to react with probe **LGP-CL** (Fig. 1c, blue and gray lines), which further confirmed the dual-lock-dual-key mechanism. Besides, CL images using the Xenogen IVIS® Spectrum imaging system in about 30 min (Fig. 1d) were collected to be consistent with the result above. As shown in Fig. 1e, the fluorescent spectra of the probe triggered by both APN and DPPIV exhibited an obvious absorption spectrum with maximum excitation and emission at 400 and 550 nm, respectively. All these results clearly demonstrated that probe **LGP-CL** could only be sequentially activated by dual proteases.

To shed light on the hydrolysis mechanism of **LGP-CL**, **GPL-CL** and its degradation intermediates, molecule docking simulations were performed through Molecular Operating Environment (Schrödinger Maestro software) [35]. The crystal structures of APN (PDB ID: 4FYR) and DPPIV (PDB ID: 1R9N) were retrieved from Protein Data Bank. The active site of APN centered on Zn^{2+} and some residues around binding pocket such as His388, Glu411, and Gln213. The active site of DPPIV centered on the catalytic triad (Ser630, Asp708, and His740). Ultimately, output 3 top-ranked poses and corresponding scores (Table S1 in Supporting information). Detail procedures and data were described in Supporting information. Based on that, we analyzed the impact of peptide sequences on catalytic distance and spatial confirmation. In Figs. 1f and g, we calculated the spatial distances between the leucine groups of **LGP-CL** and the leucine-caged CL scaffold (substrate L-CL) from the catalytic center of APN cavities, revealing distances of 6.6 and 6.2 Å, respectively. The difference in these distances was found to be insignificant, suggesting that APN exerted shearing effects on both **LGP-CL** and L-CL. In Figs. 1h and i, however, we observed that the spatial distance of **GPL-CL** from the DPPIV cavity was significantly longer at 6.5 Å compared to substrate GP-CL, which had a distance of only 3.9 Å from DPPIV catalytic centers. This discrepancy may explain why DPPIV was unable to effectively cleave probe **GPL-CL**. Notably, the chemscore values of the active sites for **LGP-CL** in APN and **GPL-CL** in DPPIV were −4.211 and −7.405 (Table S1). We assumed that this observation might be attributed to the rigid and stereospecific nature of the leucine residue, which could limit effective interactions between protease recognition sites and catalytic cavities. These findings substantially supported our hypothesis that the appropriate substrate sequence played a critical role in effective dual-protease imaging. Therefore, probe **LGP-CL** was selected in following research.

Successively, we investigated *in vitro* performance of probe **LGP-CL**. First, probe **LGP-CL** showed a good stability in room temperature with dark condition and no obvious decrease of peak area by HPLC was observed during 15 days (Figs. 2a and b). Second, we

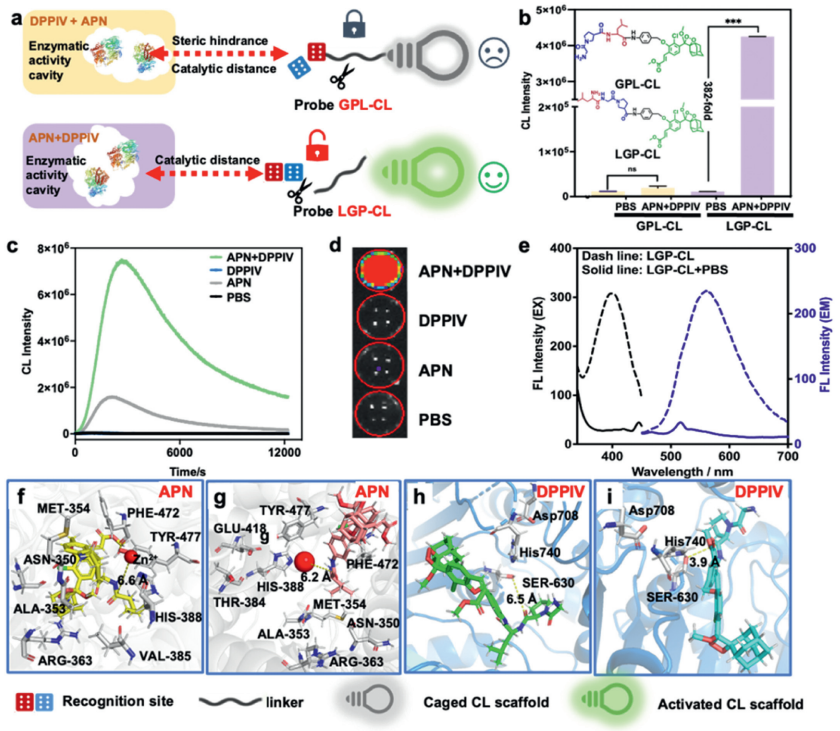

Fig. 1. (a) Design strategy for illustrating the impact of amino acid sequence on the cleavage activity of two proteases. (b) Chemical structrues of **GPL-CL** and **LGP-CL** and their CL intensity in the absence or presence of APN and DPPIV. Statistical significance was calculated *via* a two-tailed Student's *t*-test ($^{***}P < 0.001$). Data are shown as mean ± SD ($n = 3$). (c) CL kinetic curves of **LGP-CL** in the absence or presence of APN or/and DPPIV. (d) CL imaging of probe **LGP-CL** in the absence or presence of APN or/and DPPIV (30 min). (e) Fluorescent excitation and emission spectra of **LGP-CL** in the absence or presence of proteases (APN and DPPIV). (f) The binding poses of **LGP-CL** (yellow) on APN (light gray). (g) The binding poses of L-CL (pink) on APN (light gray). (h) The binding poses of **GPL-CL** (green) on DPPIV (marine). (i) The binding poses of GP-CL (cyan) on DPPIV (marine). In which, the yellow dotted lines represent the distance between the carbonyl carbon of CL probes and the catalytic active sites of proteases. Measurements conditions: 40 μmol/L **LGP-CL** in PBS, APN (100 U/L) and DPPIV (1 μg/mL).

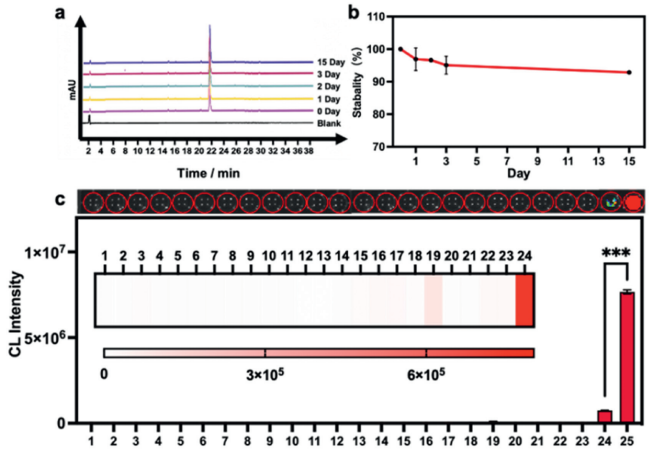

Fig. 2. *In vitro* performance. (a) HPLC spectra for stability of probe **LGP-CL**. Experimental condition: **LGP-CL** (1 mmol/L, DMSO) in dark environment at room temperature for 15 days. (b) Quantification for (a). (c) CL responses of **LGP-CL** towards different biomolecules (1. Na^+; 2. K^+; 3. Ca^{2+}; 4. Mg^{2+}; 5. Fe^{2+}; 6. Zn^{2+}; 7. H_2O_2; 8. glucose; 9. glutathione; 10. cysteine; 11. homocycteine; 12. lysine; 13. glutamic acid; 14. proline; 15. arginine; 16. alanine; 17. glutamine; 18. trypsin; 19. tyrosinase; 20. AChE; 21. CES1; 22. CES2; 23. DPPIV; 24. APN; 25. APN and DPPIV. Measurements conditions: 1 mmol/L for 1–18; 100 U/L for 19, 20, 24; 10 μg/mL for 21 and 22; 1 μg/mL for 23; 100 U/L APN + 1 μg/mL DPPIV for 25. Measurements conditions: 40 μmol/L **LGP-CL** in PBS. Statistical significance was calculated *via* a two-tailed Student's *t*-test ($^{***}P < 0.001$). Data are shown as mean ± SD ($n = 3$).

evaluated the selectivity of **LGP-CL** by introducing various potential interfering species, including metal ions, amino acids, and several proteases commonly found in biological fluids, such as tyrosinase, acetylcholinesterase (AChE), carboxyl-esterases 1 (CES1), and CES2. All species (100 μL) were added into with the same concentration of probe **LGP-CL** (40 μmol/L, 100 μL). The CL intensity were immediately recorded. As shown in Fig. 2c, the coexistence of APN and DPPIV showed significantly higher signal than those observed from APN only, DPPIV only, other proteases, and biological species. It demonstrated the high selectivity of probe **LGP-CL** for dual proteases, even in complex biological matrices. Third, our results confirmed that the observed turn-on light conversions were both APN/DPPIV concentration-dependent (Figs. S4 and S5 in Supporting information). The limits of detection (LOD) were calculated to be 0.095 U/L for APN and 0.057 ng/mL for DPPIV (3σ/slope), respectively. These findings collectively indicated that probe **LGP-CL** possesses notable advantages, including stability, selectivity, and sensitivity. These results made it a potential tool for biomarker testing.

Encouraged by the excellent properties of **LGP-CL** *in vitro*, we extended its application in cell imaging. The cytotoxicity of **LGP-CL** in HepG2 cells and LO2 cells was examined using a standard cell counting kit-8 (CCK8) assay and demonstrated to be very low, even with the concentration of **LGP-CL** up to 100 μmol/L (Fig. S6 in Supporting information).

To investigate the ability of probe **LGP-CL** to discriminate different cell lines, thus for precise diagnosis. Five cell lines (20,000 per well), including MCF-7, MCF-10a, RAW264.7, LO2, and HepG2, were seeded into 96-well plates one day before the experiment. Then, the plate was washed to remove the culture medium. Next, probe **LGP-CL** (40 μmol/L, 100 μL, dissolved in 1% DMSO) was added into each well, and the luminescence signal was immediately recorded with a Xenogen IVIS® Spectrum imaging system. As shown in Fig. 3a, CL signal produced by HepG2 cells was significantly stronger than that from other cell lines. It suggested an excellent ability to discriminate liver tumor cells from normal and other cancer cells. To further assess the quantitative capability of

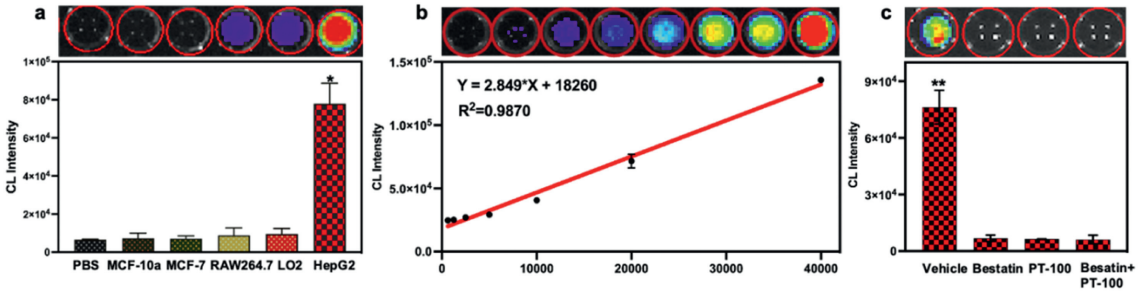

Fig. 3. Visualization of endogenous proteases in cells using probe **LGP-CL** with PBS as a control group. (a) CL images of different cell lines (20,000 cells for each well) incubated with probe **LGP-CL**. (b) CL images of different counts of HepG2 incubated with probe **LGP-CL** (0, 625, 1250, 2500, 5000, 10,000, 20,000, 40,000 cells for each well). (c) CL images of HepG2 incubated with **LGP-CL** in the absence or presence of bestatin, PT-100, the mixture of bestatin and PT-100. Measurements conditions: 40 μmol/L **LGP-CL** in PBS, bestatin (1 mmol/L) and PT-100 (100 μmol/L). Statistical significance was calculated *via* a two-tailed Student's *t*-test ($^{**}P < 0.01$). Data are shown as mean ± SD ($n = 3$).

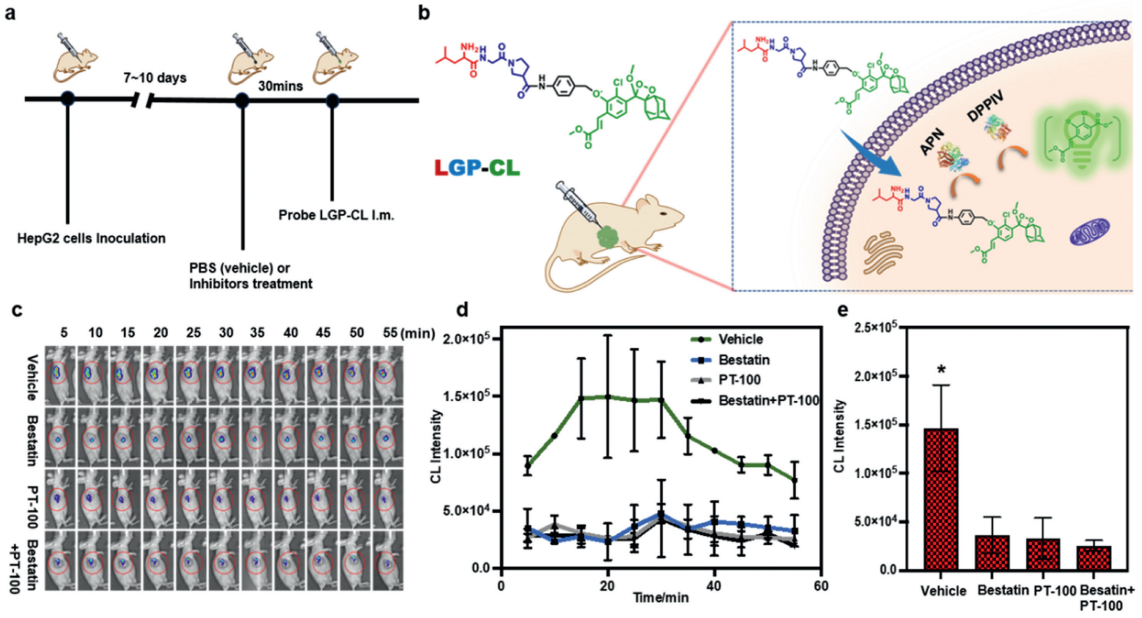

Fig. 4. Visualization of endogenous proteases in tumor-bearing mice using probe **LGP-CL**. (a) Procedures of animal experiments. (b) Proposed cartoon mechanism for CL imaging *in vivo*. (c) CL Images of tumor-bearing mice treated with probe **LGP-CL** and inhibitors in different time. (d) Quantification of part (c). (e) CL images after intratumoral injection of probe **LGP-CL** (vehicle group) or pre-injection of inhibitor bestatin (bestatin group), PT-100 (PT-100 group), and two inhibitors (bestatin + PT-100 group). Measurements: probe **LGP-CL** (50 μmol/L); Bestatin group: probe **LGP-CL** (50 μmol/L) pretreated with bestatin (500 μmol/L); PT-100 group: probe **LGP-CL** (50 μmol/L) pretreated with PT-100 (25 μmol/L); Bestatin + PT-100 group: Probe **LGP-CL** (50 μmol/L) pretreated with bestatin (500 μmol/L) and PT-100 (25 μmol/L). Statistical significance was calculated *via* a two-tailed Student's *t*-test ($^{*}P < 0.05$). Data are shown as mean ± SD ($n = 3$).

probe **LGP-CL**, we examined its linearity between CL signal and cell counts. As depicted in Fig. 3b, CL intensity exhibited an anticipated increase with cell counts, showing a robust linear relationship within the range of 625–40,000 cells ($R^2 = 0.9870$). These results demonstrated that probe **LGP-CL** could easily penetrate cell membrane and indicate the level of endogenous APN and DPPIV efficiently in living cells. To further specify that the "turn-on" CL signal was caused by intracellular APN and DPPIV, the cells were pretreated with the inhibitors (bestatin, PT-100 and the mixture) for 30 min prior to the addition of probe **LGP-CL**. The resulting declined CL signal by pretreated cells confirmed that the obvious CL enhancement was mainly specific to dual-protease-mediated light emission of **LGP-CL** (Fig. 3c).

Subsequently, we examined the capacity of probe **LGP-CL** to visualize endogenous proteases in tumor-bearing mice. All animal studies in this work were approved in compliance with guidelines of Institutional Animal Care and Use Committee of School of Pharmacy, Fudan University. As shown in Fig. 4a, the 6-week-old BALB/c nude mice were inoculated with 2.5×10^6 HepG2 cells under the skin of the right hind limb. When the tumor size was up to about 100 mm^3, tumor bearing mice were divided into four groups randomly and anesthetized with 3% isoflurane in 97% oxygen gas. Three groups were treated with 100 μL of bestatin (500 μmol/L), PT-100 (25 μmol/L), both bestatin (500 μmol/L) and PT-100 (25 μmol/L) with the other group treated with phosphate buffered saline (PBS) as the control group (vehicle) for 1 h. CL images were recorded immediately after the administration of 50 μL probe **LGP-CL** (50 μmol/L) through intra-tumoral injection. As illustrated in Fig. 4b, CL signals generated from the controlled removal of leucine and glycine-proline residues after treating probe **LGP-CL**. From CL images in Figs. 4c and d, the CL signal increased immediately after the administration of probe **LGP-CL** and reached the highest about 20–30 min. As shown in Fig. 4e, robust CL signals were observed in the **LGP-CL** treated mice (vehicle), higher than that from the inhibitor-pretreated groups, which validated that the observed "turn-on" CL signal was indeed a result of the activity of both proteases and could be inhibited by either bestatin or PT-100. These findings provided compelling evidence that probe **LGP-CL** could effectively visualize the upregulation of dual proteases at tumor sites.

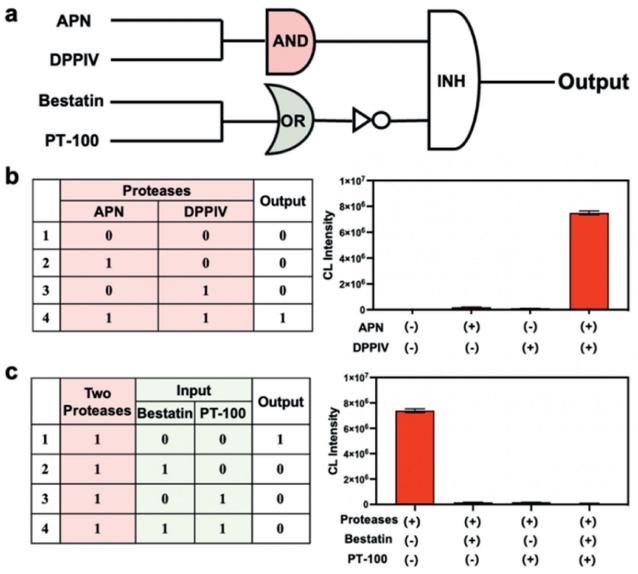

Fig. 5. Modular device engineering with probe **LGP-CL**. (a) An integrated logic gate built by probe **LGP-CL**, proteases and their inhibitors. (b) The truth table for "AND" logic gate and CL intensity of **LGP-CL** triggered by proteases. (c) The truth table for "OR" and "INH" logic gates and CL intensity of **LGP-CL** in the presence of proteases and their inhibitors. Measurement conditions: **LGP-CL**: 40 μmol/L; APN: 100 U/L; DPPIV: 1 μg/mL; bestatin: 1 mmol/L; PT-100: 100 μmol/L. Data are shown as mean ± SD ($n = 3$).

Futhermore, the newly developed CL probe provided an opportunity to engineer modular devices [36] in a programmable way. As shown in Fig. 5a, APN and DPPIV were firstly employed as two inputs in the system to modulate CL output. In the truth table (Fig. 5b), we defined the presence of two protease inputs as "1", and the absence as "0". An elevated CL intensity was defined as output "1", and no obvious signal change as output "0". In the case of no input, no CL emission was observed (output "0"). With a single input (Fig. 5b), neither APN nor DPPIV showed obvious CL signal (output "0"). However, the significantly enhanced CL signal (output "1") was triggered to emit in the presence of both APN and DPPIV, which led to "AND" logic circuit. Subsequently, we added the inhibitors to further establish the "OR" and "INHIBIT" logic gates. With the presence of two proteases, the selective inhibitors (bestatin for APN, PT-100 for DPPIV respectively) were employed to validate their inhibition effects. We defined the presence of inhibitor inputs as "1" and the absence as "0". It was still specified that CL intensity was defined as output "1", and no significant signal as output "0". As shown in Fig. 5c, either or both of bestatin and PT-100 resulted the significant suppression of CL signal (output "0"), which was consistent with "OR" and "INH" logic gates. Thus, an integrated molecular logic gate computation was established by using two proteases and their inhibitors to tune the light of a unimolecular probe.

In summary, we have successfully designed a unimolecular dual-locked CL probe, denoted as **LGP-CL**, offering a sensitive and rapid alternative for imaging the upregulation of dual proteases both *in vitro* and in living systems. The design of cage group was demonstrated to be essential for efficient and specific dual-protease detection. Probe **LGP-CL** enabled the excellent "dual-lock-dual-key" fit with a 382-fold enhancement of CL emission while the energy of probe **GPL-CL** was still caged without light emission. By virtue of its good stability, selectivity and cell viability, **LGP-CL** also allows for upregulated dual-protease imaging in liver tumor cells and tumor-bearing mice. Particularly, the obvious difference in CL signal to various cell lines confirms its potential for distinguishing liver tumor cells (HepG2) from LO2, MCF-7, MCF-10a and RAW264.7. Overall, the newly developed CL probe with cascaded activation mechanism may facilitate rapid investigation into the role played by proteases in liver diseases, and enabling the timely selection of appropriate treatment. We anticipate that our work not only sheds light on the rational design of optical probes for dual-protease imaging, but provides a promising tool for clinical diagnosis precisely, drug discovery, and simply engineering an integrated logic gates (AND, OR and INHIBIT).

Declaration of competing interest

The authors declare no competing financial interests or personal relationships that could have appeared to influence the work reported in this paper.

Acknowledgments

We acknowledge the financial support by National Key R&D Program of China, MOST (No. 2023YFC2510000), Shanghai Science and Technology (No. 21N31900500), Shanghai Municipal Health Commission Project (No. 202140016), Training Program for Outstanding Young Medical and Pharmaceutical Talents of Minhang District Health System (No. mwyjyx08) and the Project of Basic Medicine funded by Fudan-Minhang Health Consortium (Nos. 2021MHJC10 and 2023FM09).

Supplementary materials

Supplementary material associated with this article can be found, in the online version, at doi:10.1016/j.cclet.2024.109784.

References

[1] O. Vasiljeva, D.R. Hostetter, S.J. Moore, et al., Biol. Chem. 400 (2019) 965–977.
[2] J.S. Bond, J. Biol. Chem. 294 (2019) 1643–1651.
[3] N. Guyot, J. Wartelle, L. Malleret, et al., Am. J. Pathol. 184 (2014) 2197–2210.
[4] Y. Han, S. Ma, Q. Zhang, Chin. Chem. Lett. 34 (2023) 107589.
[5] K. Pan, K. Ohnuma, C. Morimoto, et al., Cureus 13 (2021) 13495.
[6] F. Chen, J. Wang, Y. Wu, et al., Front. Oncol. 12 (2022) 822449.
[7] L. Wu, J. Huang, K. Pu, T.D. James, Nat. Rev. Chem. 5 (2021) 406–421.
[8] M. Zhai, Z. Yang, C. Zhang, et al., Cell Death Dis. 11 (2020) 396.
[9] X. Zhang, W. Xu, Curr. Med. Chem. 15 (2008) 2850–2865.
[10] M. Itou, T. Kawaguchi, E. Taniguchi, M. Sata, World J. Gastroenterol. 19 (2013) 2298–2306.
[11] M.T. Nguyen, T. Van Kersavond, S.H. Verhelst, ACS Chem. Biol. 10 (2015) 2423–2434.
[12] A.P. Soleimany, C. Martin-Alonso, M. Anahtar, et al., ACS Omega 7 (2022) 24292–24301.
[13] H. Pan, X. Chai, J. Zhang, Chin. Chem. Lett. 34 (2023) 108321.
[14] J.I. Scott, Q. Deng, M. Vendrell, ACS Chem. Biol. 16 (2021) 1304–1317.
[15] S. Chakrabarty, JP. Kahler, MAT. van de Plassche, et al., Curr. Top. Microbiol. Immunol. 420 (2019) 253–281.
[16] J. Huang, J. Li, Y. Lyu, et al., Nat. Mater. 18 (2019) 1133–1143.
[17] Q.J. Duan, Z.Y. Zhao, Y.J. Zhang, et al., Adv. Drug Deliv. Rev. 196 (2023) 114793.
[18] X. He, L. Li, Y. Fang, et al., Chem. Sci. 8 (2017) 3479–3483.
[19] X. Guo, S. Mu, J. Li, et al., J. Mater. Chem. B 8 (2020) 767–775.
[20] L. Feng, Z. Tian, M. Zhang, et al., Chin. Chem. Lett. 32 (2021) 3053–3056.
[21] Y. Ren, Y. Qiang, B. Zhu, et al., Anal. Chem. 93 (2021) 4334–4341.
[22] F. Huan, Q. Meng, H.T. Ta, et al., New J. Chem. 44 (2020) 12890–12896.
[23] J. Zhan, F. Shi, F. Shi, et al., Chin. Chem. Lett. 34 (2023) 108791.
[24] C. Liu, R. Zhang, W. Zhang, et al., J. Am. Chem. Soc. 141 (2019) 8462–8472.
[25] Y. Li, W. Wu, J. Yang, et al., Chem. Sci. 7 (2016) 1920–1925.
[26] H. Peng, T. Wang, G. Li, et al., Anal. Chem. 94 (2022) 1070–1075.
[27] J. Boo, J. Lee, YH. Kim, et al., Front. Chem. 11 (2023) 1133018.
[28] R. Blau, O. Shelef, D. Shabat, et al., Nat. Rev. Bioeng. 1 (2023) 648–664.
[29] U. Haris, A.R. Lippert, ACS Sens. 8 (2023) 3–11.
[30] S. Gutkin, O. Green, G. Raviv, et al., Bioconjug. Chem. 31 (2020) 2488–2493.
[31] N. Hananya, O. Press, A. Das, et al., Chemistry 25 (2019) 14679–14687.
[32] A. Fu, Y. Mao, H. Wang, et al., J. Pharm. Biomed. Anal. 204 (2021) 114266.
[33] A. Fu, H. Wang, T. Huo, et al., Anal. Chem. 93 (2021) 6501–6507.
[34] R. Sun, X. Wu, Y. Mao, et al., Luminescence 37 (2022) 1335–1342.
[35] L. Ivanova, J. Tammiku-Taul, A.T. García-Sosa, et al., ACS Omega 3 (2018) 11407–11414.
[36] P.A. de Silva, N.H.Q. Gunaratne, C.P. McCoy, Nature 364 (1993) 42–44.